DOI: 10.3901/CJME.2015.0114.015, available online at www.springerlink.com; www.cjmenet.com; www.cjme.com.cn

Approximate-model Based Estimation Method for Dynamic Response of Forging Processes

LEI Jie, LU Xinjiang*, LI Yibo, HUANG Minghui, and ZOU Wei

State Key Laboratory of High Performance Complex Manufacturing, Central South University, Changsha 410083, China

Received July 21, 2014; revised December 10, 2014; accepted January 14, 2015

Abstract: Many high-quality forging productions require the large-sized hydraulic press machine (HPM) to have a desirable dynamic response. Since the forging process is complex under the low velocity, its response is difficult to estimate. And this often causes the desirable low-velocity forging condition difficult to obtain. So far little work has been found to estimate the dynamic response of the forging process under low velocity. In this paper, an approximate-model based estimation method is proposed to estimate the dynamic response of the forging process under low velocity. First, an approximate model is developed to represent the forging process of this complex HPM around the low-velocity working point. Under guaranteeing the modeling performance, the model may greatly ease the complexity of the subsequent estimation of the dynamic response because it has a good linear structure. On this basis, the dynamic response is estimated and the conditions for stability, vibration, and creep are derived according to the solution of the velocity. All these analytical results are further verified by both simulations and experiment. In the simulation verification for modeling, the original movement model and the derived approximate model always have the same dynamic responses with very small approximate error. The simulations and experiment finally demonstrate and test the effectiveness of the derived conditions for stability, vibration, and creep, and these conditions will benefit both the prediction of the dynamic response of the forging process and the design of the controller for the high-quality forging. The proposed method is an effective solution to achieve the desirable low-velocity forging condition.

Keywords: performance analysis, forging process, modeling, hydraulic press machine

1 Introduction

The large-sized hydraulic press machine (HPM) is a crucial piece of equipment in industry. Its purpose is to forge a metal work piece to form a desirable shape in the dies. Generally, many high-quality productions need an isothermal forging[1–2], which is usually required to work under a desirable low-velocity condition. This condition depends on the dynamic response of the HPM. Thus, the estimation of the dynamic response of the HPM is very important to the high-quality forging.

As the strength and size of a work piece increase, the deformation force becomes huge, which leads to a huge driving force from the HPM for forging[3–4]. This makes the forging process to involve many complex behaviors at low velocity. First, the deformation force of a work piece is complex[5–7]. On the one hand, since the shape of the work piece is often irregular, this leads to an irregular deformation during forging. This irregular deformation will produce a complex deformation force of the work piece. On the other hand, there is a complex influence from the material property, stress, stress ratio, and temperature on this deformation force. Second, the coupling between mechanism dynamics and hydraulic dynamics are inevitable due to mutually transfer of both motion and force between the mechanism system and the hydraulic system[8]. Furthermore, the friction force is inevitable and its model is also complex at the low velocity[8–12]. All aforementioned factors bring a big challenge for the estimation of the dynamic response of the HPM.

Little work has been contributed to the estimation of the dynamic response of the hydraulic equipments, except via experiment[13–15] and simulation[15–16]. But they lack generality since these results are only effective for their special conditions. They also never pay attention to the conditions of stable run, vibration, and creep. In other fields, many researchers have contributed to estimate the friction influence on the velocity vibration and creep[17–19]. However, their results are difficult to extend to this complex forging process. Further, little work was found to analyze the influence of the friction and the deformation force of the work piece on the dynamic response of the complex forging process, except Refs. [16, 20]. But Refs. [16, 20] are only from simulation to estimate this influence, whose results are only effective for their special conditions.

* Corresponding author. E-mail: luxj@csu.edu.cn
Supported by National Basic Research Program of China(973 Program, Grant No. 2011CB706802), National Natural Science Foundation of China (Grant No. 51205420), Program for New Century Excellent Talents in University of China(Grant No. NCET-13-0593), and Hunan Provincial Natural Science Foundation of China(Grant No. 14JJ3011)

Thus, it is still necessary to estimate the dynamic response of this complex forging process.

In this paper, an approximate-model based estimation method is proposed to estimate the dynamic response of the HPM around the low-velocity working point. First, an approximate model is developed to approximate this complex HPM system around the working point. On this basis, the conditions for stability, vibration, and creep are derived. All analytical results are further verified by both simulations and experiment.

2 Modeling of the HPM

The HPM studied in this paper is shown in Fig. 1. This hydraulic press system includes three driving cylinders and four return cylinders, which are located above and below the work plate respectively in order to drive the movement of the work plate. These cylinders are driven by their corresponding hydraulic systems, which consist of pumps, valves, and pipes. A control system is also required to adjust the servo valve of the hydraulic system to achieve a desirable velocity for the work plate to have the high-quality forging.

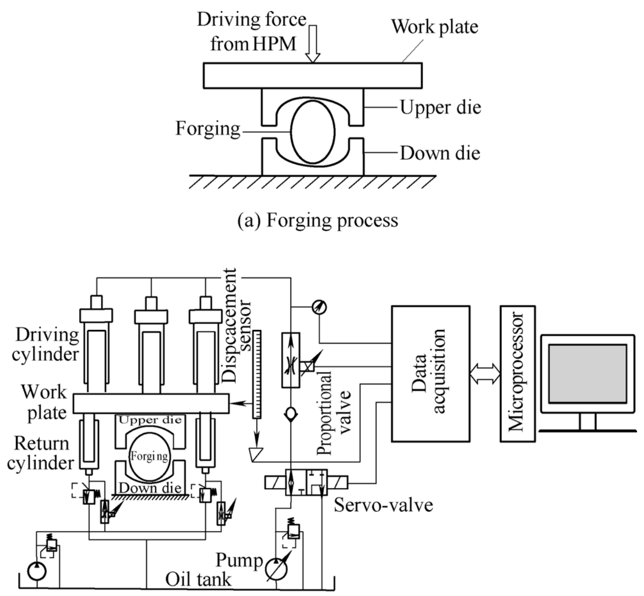

(a) Forging process

(b) Simplified driven system and control system

Fig. 1. Diagram of the HPM

2.1 Dynamics of the forging process

According to the Newton's second law, the movement model of the work plate is the following:

$$M\frac{\mathrm{d}^2x}{\mathrm{d}t^2}+B\frac{\mathrm{d}x}{\mathrm{d}t}=F_d-F_Z-F_2-F_f+Mg, \tag{1}$$

where M is the mass of both the work plate and all hydraulic cylinders respectively, and x is the displacement of the work plate, B is the viscous damping coefficient at the guide pillar and the cylinder seal, F_d is the driven force from the driven cylinders, F_Z is the deformation force of the work piece, F_2 is the support force from the return cylinders and may be regarded as a constant value, F_f is the friction at the piston-cylinder seal and guide, g is the acceleration of gravity.

The driving force model of the hydraulic cylinder can be represented by[21]

$$\begin{aligned} F_d &= Ap, \\ Q &= A\frac{\mathrm{d}x}{\mathrm{d}t}+\frac{V_0+Ax}{\beta_e}\frac{\mathrm{d}p}{\mathrm{d}t}, \end{aligned} \tag{2}$$

where Q is the flow, p is the pressure, A is the area sum of all hydraulic cylinders, V_0 is the initial volume, β_e is the spring moment of medium.

The deformation force of a work piece is complex. It is a function of the displacement x, velocity v of the work plate, and the shape, material, and temperature of the work piece. For example, a long rectangular work piece with the Rosserd material model for aluminum alloy is expressed as[5–7, 20]

$$\begin{aligned} F_Z &= \frac{V}{h}\left(\frac{2}{\sqrt{3}}+\mu_S\frac{V}{2lh^2}\right)\sigma_S, \\ \sigma_S &= c\varepsilon^n\dot{\varepsilon}^m+y, \end{aligned} \tag{3}$$

where a, h, l are the width, the height, and the length of this forging respectively, $V=ahl$ is the volume, μ_s is the friction coefficient between the forging and the dies, σ_S is the flow stress, the parameters c, n, m, and y depend on the material and the temperature, $\varepsilon=x/h$ and $\dot{\varepsilon}=v/(h-x)$ are the strain and the strain rate respectively, v is the velocity of the work plate.

A well-known friction model is the Stribeck friction model since it is a well representation of the dynamic behavior of the friction at low velocity[20]. Its equation is as below:

$$F_f=(F_c+\sigma_2 v)+(F_s-F_c)\exp\left(-\left(\frac{v}{v_s}\right)^2\right), \tag{4}$$

where F_c and F_s are the Coulomb and static friction values, v_s and σ_2 are the Stribeck velocity and the friction coefficient respectively.

2.2 Approximate model

Obviously, the dynamics of the forging process represented by Eqs. (1)–(4) is complex, which is difficult to solve analytically. To ease the complexity of the dynamic response estimation, an approximate model is developed. This developed model will also be easily used to design the controller.

The forging distances of many work pieces are much smaller compared to the whole stroke of the work plate, which makes the volume Ax caused by their deformation quite smaller than the initial volume V_0. In these real conditions, the driving force (Eq. (2)) may be approximated by

$$AQ \approx A^2 v + \frac{V_0}{\beta_e}\frac{\mathrm{d}F_d}{\mathrm{d}t}. \tag{5}$$

The integral of Eq. (5) gives the following:

$$F_d = k_d t - k_x x + C_0, \tag{6}$$

where $k_d = AQ\beta_e / V_0$, $k_x = A^2\beta_e / V_0$, C_0 is constant.

Then, at a small forging distance, the deformation force may be also simplified as a linear function of the displacement x and the velocity v

$$F_Z = K_{zx}x + K_{zv}v + F_0, \tag{7}$$

where the parameters K_{zx}, K_{zv} and F_0 may be obtained from the Taylor expansion via the deformation force model, such as Eq. (3), or via data identification. For a long rectangular work piece with the Rosserd material model for aluminum alloy, these parameters at the working point (x=x_0, v=v_0) can be expressed as follows:

$$F_0 = \frac{V}{h}\left(\frac{2}{\sqrt{3}} + \mu_s \frac{V}{2lh^2}\right)\left[c\left(\frac{x_0}{h}\right)^n\left(\frac{v_0}{h - x_0}\right)^m + y\right],$$

$$K_{zx} = \frac{V}{h}\left(\frac{2}{\sqrt{3}} + \mu_s \frac{V}{2lh^2}\right)ch^{-n-m}v_0^m \times \left[nx_0^{n-1}\left(1 - \frac{x_0}{h}\right)^{-m} + h^{-1}mx_0^n\left(1 - \frac{x_0}{h}\right)^{-m-1}\right],$$

$$K_{zv} = \frac{V}{h}\left(\frac{2}{\sqrt{3}} + \mu_s \frac{V}{2lh^2}\right)cm\left(\frac{x_0}{h}\right)^n (h - x_0)^{-m} v_0^{m-1}.$$

We also approximate the Stribeck friction model (4) with a linear model at the working point v=v_0:

$$F_f = \varphi_1 + \varphi_2 v, \tag{8}$$

where

$$\varphi_1 = F_c + (F_s - F_c)\left(1 + \frac{2v_0^2}{v_s^2}\right)\exp\left(-\left(\frac{v_0}{v_s}\right)^2\right),$$

$$\varphi_2 = \sigma_2 - (F_s - F_c)\frac{2v_0}{v_s^2}\exp\left(-\left(\frac{v_0}{v_s}\right)^2\right).$$

Inserting Eqs.(6–8) into Eq. (1), the dynamic model of the HPM is rewritten as:

$$M\frac{\mathrm{d}^2x}{\mathrm{d}t^2} + (B + \varphi_2 + K_{zv})\frac{\mathrm{d}x}{\mathrm{d}t} + (K_{zx} + k_x)x = k_d t + Mg - \varphi_1 - F_0 - F_2 + C_0. \tag{9}$$

Define

$$\xi = \frac{B + \varphi_2 + K_{zv}}{2\sqrt{M(K_{zx} + k_x)}},\ \omega_n = \sqrt{\frac{K_{zx} + k_x}{M}}, \tag{10}$$

where ξ and ω_n are the damping ratio and the natural frequency respectively. Eq. (9) may be rewritten as

$$\ddot{x} + 2\xi\omega_n\dot{x} + \omega_n{}^2 x = \frac{k_d t}{M} + \frac{\Delta F}{M}, \tag{11}$$

where $\Delta F = Mg - \varphi_1 + C_0 - F_0 - F_2$. Its solution can be easily derived as follows.

When $0 \leqslant \xi < 1$,

$$x(t) = \frac{k_d}{K_{zx} + k_x}t - \frac{(B + \varphi_2 + K_{zv})k_d}{(K_{zx} + k_x)^2} + \frac{\Delta F}{K_{zx} + k_x} + \exp(-\xi\omega_n t)(C_1\cos\omega_d t + C_2\sin\omega_d t). \tag{12}$$

When $\xi > 1$,

$$x(t) = \frac{k_d}{K_{zx} + k_x}t - \frac{(B + \varphi_2 + K_{zv})k_d}{(K_{zx} + k_x)^2} + \frac{\Delta F}{K_{zx} + k_x} + C_3\exp(r_1 t) + C_4\exp(r_2 t). \tag{13}$$

When $\xi = 1$,

$$x(t) = \frac{k_d}{K_{zx} + k_x}t - \frac{(B + \varphi_2 + K_{zv})k_d}{(K_{zx} + k_x)^2} + \frac{\Delta F}{K_{zx} + k_x} + (C_5 + C_6 t)\exp(r_3 t), \tag{14}$$

where $r_{1,2} = -\xi\omega_n \pm \omega_n\sqrt{\xi^2 - 1}$, $r_3 = -\omega_n$, $\omega_d = \omega_n\sqrt{1 - \xi^2}$, and the parameters C_1, C_2, C_3, C_4, C_5 and C_6 can be decided according to the initial conditions. For example, inserting the initial conditions $x(0)$ and $v(0)$ into Eq. (12), we have

$$C_1 = x(0) + \frac{(B + \varphi_2 + K_{zv})k_d}{(K_{zx} + k_x)^2} - \frac{\Delta F}{K_{zx} + k_x},$$

$$C_2 = \frac{v(0)}{\omega_d} - \frac{k_d}{\omega_d(K_{zx} + k_x)} + \frac{\xi\omega_n}{\omega_d}\left[x(0) + \frac{(B + \varphi_2 + K_{zv})k_d}{(K_{zx} + k_x)^2} - \frac{\Delta F}{K_{zx} + k_x}\right]. \tag{15}$$

Since these solutions include the exponential term and the sinusoidal term, it is difficult to directly estimate the velocity response.

3 Estimation of Velocity Response

In this section, the dynamic responses of the forging process will be estimated from three aspects.

3.1 When $0 \leqslant \xi < 1$

Differentiating Eq. (12), we have

$$v(t) = \frac{k_d}{K_{zx} + k_x}[1 - J_0 \exp(-\xi\omega_n t)\sin(\omega_d t + \psi)], \tag{16}$$

where ψ and J_0 may be derived from Eq. (12). The following two cases will be discussed.

3.1.1 When $\xi=0$

The system velocity may be rewritten as

$$v(t) = \frac{k_d}{K_{zx} + k_x}[1 - J_0 \sin(\omega_d t + \psi)]. \tag{17}$$

From Eq. (17), the velocity will have an undamped oscillation. When J_0 is larger than one, the system will appear creep since the velocity may be equal to zero.

3.1.2 When $0<\xi<1$

Obviously, from Eq. (16), the velocity response is fully dependent on the product of the exponential term and the sinusoidal term. Since the term $\xi\omega_n$ is larger than zero, the exponential term converges to zero as $t = \infty$. This means the system can run in a stable configuration and the final velocity v_∞ is equal to $k_d/(K_{zx}+k_x)$.

Of course, the velocity v will fluctuate before converging to the final velocity v_∞. To make a prediction of the dynamic response, the maximal overshoot of the velocity should be estimated. The velocity v reaches its maximal value when $\sin(\omega_d t+\psi)=1$ due to two reasons:

(1) Since the frequency ω_d is large, the maximal value of the sinusoidal term is taken at near zero time.

(2) The exponential term reduces with time and reaches its maximal value at the zero time.

So the required time of the maximal overshoot may be estimated as

$$t_0 = \frac{3\pi/2 - \psi}{\omega_d} \quad \text{or} \quad t_0 = \frac{\pi/2 - \psi}{\omega_d}. \tag{18}$$

When $t_0 = (3\pi/2 - \psi)/\omega_d$, the maximal overshoot is larger than v_∞ and may be calculated as

$$v_{\max}^p = \frac{k_d}{K_{zx} + k_x}[1 + J_0 \exp(-\xi\omega_n t_0)]. \tag{19}$$

When $t_0 = (\pi/2 - \psi)/\omega_d$, the maximal overshoot is smaller than v_∞ and may be calculated as

$$v_{\max}^n = \frac{k_d}{K_{zx} + k_x}[1 - J_0 \exp(-\xi\omega_n t_0)]. \tag{20}$$

If $v_{\max}^n > 0$, then the system will not appear creep. Otherwise, it will appear creep.

3.2 When $\xi>1$

Differentiating Eq. (13), we have

$$v(t) = \frac{k_d}{K_{zx} + k_x} + C_3 r_1 \exp(r_1 t) + C_4 r_2 \exp(r_2 t). \tag{21}$$

Since r_1 and r_2 are smaller than zero, the system can run in a stable configuration and the final velocity v_∞ is equal to $k_d/(K_{zx}+k_x)$ as $t = \infty$. Thus, when $\xi>1$, the system can also run stably.

Then, differentiating Eq. (21), we have

$$\frac{\mathrm{d}v(t)}{\mathrm{d}t} = C_3 r_1^2 \exp(r_1 t) + C_4 r_2^2 \exp(r_2 t) = \exp(r_1 t)[C_3 r_1^2 + C_4 r_2^2 \exp((r_2 - r_1)t)]. \tag{22}$$

The extreme of the velocity is gained at

$$t_0 = \frac{1}{r_2 - r_1}\ln\left(-\frac{C_3 r_1^2}{C_4 r_2^2}\right),$$

that is calculated from $\mathrm{d}v(t)/\mathrm{d}t = 0$.

If $0 \leqslant t_0 < \infty$, that is $-C_3 r_1^2 \geqslant C_4 r_2^2$, the minimal velocity is obtained by

$$v_{\min} = \min[v(t_0), v(0), v(\infty)]. \tag{23}$$

If $t_0<0$, that is $0 < -C_3 r_1^2/(C_4 r_2^2) < 1$, $\mathrm{d}v(t)/\mathrm{d}t$ is a monotonic increasing function when $t>0$. Thus, the minimal velocity is obtained by

$$v_{\min} = v(0). \tag{24}$$

If $t_0 = \infty$, that is $C_4=0$, the minimal velocity is $v_{\min} = v(0)$ due to the monotone increasing function of Eq. (21) when $C_3<0$. When $C_3>0$, then minimal velocity is $v_{\min} = v(\infty)$ due to the monotone decreasing function of Eq. (21).

Thus, when the minimal velocity is smaller than zero, the system will appear creep. Otherwise, it will not appear creep.

3.3 When $\xi=1$

Differentiating Eq. (14), we have

$$v(t) = \frac{k_d}{K_{zx} + k_x} - (C_5\omega_n - C_6 + C_6\omega_n t)\exp(-\omega_n t). \tag{25}$$

According to the limit theorem, the system will converge to a constant velocity and this final velocity may be expressed as $v_\infty = k_d/(K_{zx}+k_x)$. Then, differentiating Eq. (25), we have

$$\frac{\mathrm{d}v(t)}{\mathrm{d}t} = \omega_n \exp(-\omega_n t)(C_5\omega_n - 2C_6 + C_6\omega_n t). \qquad (26)$$

The extreme of the velocity is gained at $t_0 = (2C_6 - C_5\omega_n)/C_6\omega_n$ that is calculated from $\mathrm{d}v(t)/\mathrm{d}t = 0$. Similarly, the minimal velocity is obtained by

$$v_{\min} = \min[v(t_0), v(0), v(\infty)]. \qquad (27)$$

Thus, when the minimal velocity is smaller than zero, the system will appear creep. Otherwise, it will not appear creep.

4 Simulation and Experiment Verification

Both simulation and experiment are used to check the validity of the analytical results.

4.1 Simulation verification

The basic parameters of the HPM in the simulations are set as {F_s=11 742.98 N, F_c=10 419.54 N, σ_2=82 298.41 N/(m • s^{-1}), V_0=3 m^3, β_e=0.7×10^9 N/m^2, B=6.85×10^5 N/(m • s^{-1}), M=54 474 kg, A=0.53 m^2, l=500 mm, a=50 mm, h=44 mm}.

4.1.1 Model verification

In this model verification, a long rectangular work piece is forged. Its material is aluminum alloy (AL-1100) and the deformation force model is represented by Eq. (3). The original system (Eqs. (1)–(4)) is used to verify the approximate model (11). As shown in Fig. 2, under different forging conditions, both the original system and the approximate model always have the same dynamic responses, due to very small approximate error. Thus, this modeling is effective.

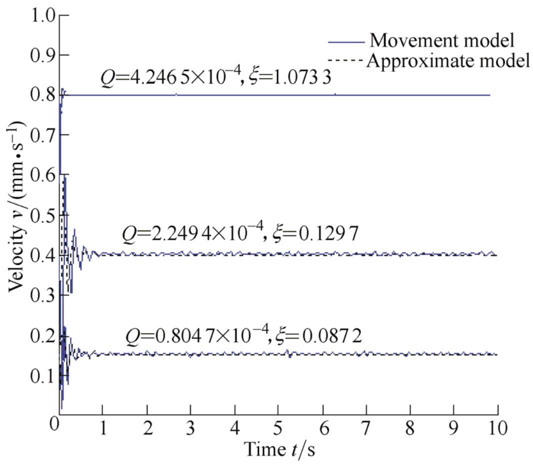

Fig. 2. Comparison of modeling performance

4.1.2 Verification of estimation performance

In the following verifications, all simulations are conducted on the original system (Eqs. (1)–(4)). Then, these simulations are used to verify the analysis results on section 3. The simulation parameters are set to satisfy the conditions derived in the section 3.

(1) Result verification at ξ=0

The other simulation parameters are set as {$x(0)$=0, $v(0)$=0.01×10^{-3} m/s, $F_d(0)$=0.886×10^5 N, v_s=0.450 938×10^{-3} m/s, F_2=1.389 8×10^5 N, Q=0.409 34×10^{-4} m^3/s, n=2.5, u_s=0.8, c=2.327 1, y=11.998 9, m=0.13}. By calculation, ξ and J_0 are equal to 0 and 1.022 6. Thus, according to the analysis result in section 3(A), the system should appear undamped oscillation and creep. Also, the mean velocity is estimated equal to 0.06 mm/s. These points will be further verified with the simulation using these actual parameters. The simulation result is shown in Fig. 3. From this figure, it is clear that the system appears undamped oscillation and creep (v=0 in the circle), and the mean velocity is equal to 0.061 mm/s. This proves the effectiveness of the condition of the undamped oscillation and creep.

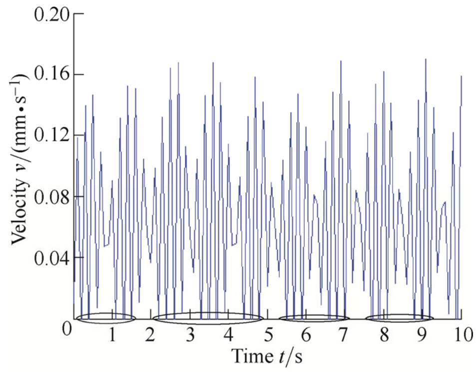

Fig. 3. Undamped oscillation and creep at ξ=0

(2) Result verification at 0<ξ<1

Two cases are used to check the result derived at 0<ξ<1. At the case 1, the simulation parameters are set as {$x(0)$=0, $v(0)$=0.011×10^{-3} m/s, $F_d(0)$=0.886 5×10^5 N, v_s=0.8×10^{-3} m/s, F_2=1.550 5×10^5 N, Q=0.359 95×10^{-4} m^3/s, n=2.2, u_s=0.85, c=4.194 8, m=0.14, y=11.392}. By calculation, ξ is equal to 0.718 6, and the final velocity and the minimal velocity are predicted equal to 0.05 mm/s and −0.001 mm/s, respectively. Thus, according to the analysis result in section 3(A), the system should run stably and appear creep. These points will be further verified with the simulation using these actual parameters. This simulation result is shown in Fig. 4, which shows that the system can run stably and appear creep, and the final velocity and the minimal velocity are equal to 0.051 mm/s and 0 mm/s. This proves the effectiveness of the condition of the stable run and creep.

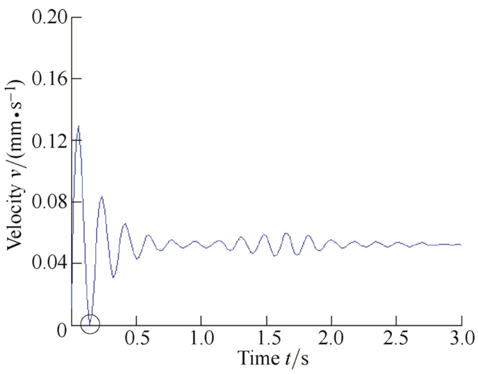

Fig. 4. Stable run and creep at $0<\xi<1$

At case 2, the simulation parameters are set as $\{x(0)=0$, $v(0)=0.01\times10^{-3}$ m/s, $F_d(0)=0.886\ 7\times10^{5}$ N, $v_s=1\times10^{-3}$ m/s, $F_2=1.344\ 75\times10^{5}$ N, $Q=1.163\ 1\times10^{-4}$ m^3/s, $n=2.4$, $u_s=0.6$, $c=1.677\ 7$, $m=0.15$, $y=13.018\ 8\}$. By calculation, ξ is equal to 0.505 9, and the final velocity and the maximal overshoot are predicted equal to 0.2 mm/s and 0.32 mm/s respectively. Thus, according to the analysis in section 3, the system should run stably and does not appear creep. These points will be further verified with the simulation using these actual parameters. This simulation result is shown in Fig. 5, which shows that the system can run stably and the final velocity and the maximal overshoot are equal to 0.2 mm/s and 0.35 mm/s. This proves the effectiveness of the condition of a stable run.

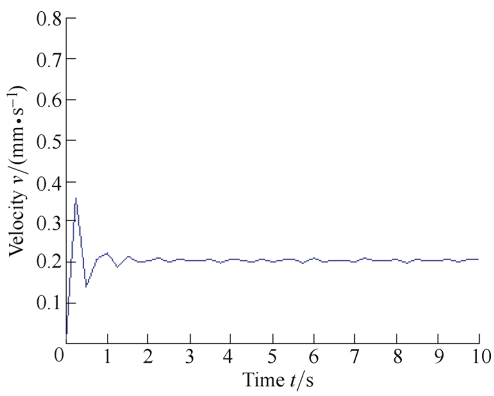

Fig. 5. Stable run at $0<\xi<1$

(3) Result verification at $\xi>1$

The simulation parameters are set as $\{x(0)=0$, $v(0)=0.08\times10^{-3}$ m/s, $F_d(0)=1.1\times10^{5}$ N, $v_s=1.8\times10^{-3}$ m/s, $F_2=1.33\times10^{5}$ N, $Q=1.718\times10^{-4}$ m^3/s, $n=2.4$, $u_s=0.75$, $c=1.069$, $m=0.1$, $y=12.89\}$. By calculation, ξ is equal to 1.133 1, and the final velocity and the maximal overshoot are predicted equal to 0.3 mm/s and 0.351 mm/s, respectively. Thus, according to the analysis in section 3(B), the system may run stably and does not appear creep. This point will be further verified with the simulation using these actual parameters. This simulation result is shown in Fig. 6. From this figure, it is clear that the system runs stably, and the final velocity and the maximal overshoot are equal to 0.301 mm/s and 0.36 mm/s, respectively.

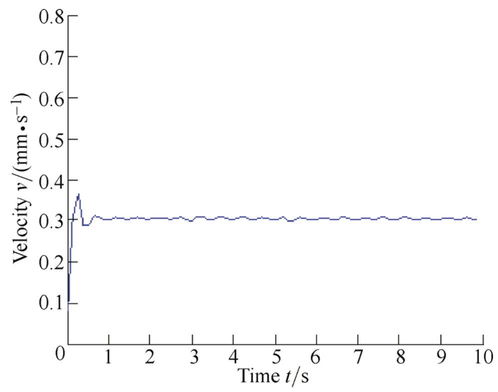

Fig. 6. Stable run at $\xi>1$

Another simulation parameters are set as $\{x(0)=0$, $v(0)=0.025\times10^{-3}$ m/s, $F_d(0)=1.196\times10^{5}$ N, $v_s=1.2\times10^{-3}$ m/s, $F_2=1.325\ 3\times10^{5}$ N, $Q=0.650\ 87\times10^{-4}$ m^3/s, $n=2.4$, $u_s=0.9$, $c=1.133$, $m=0.1$, $y=12.473\}$. By calculation, ξ is equal to 1.252 7, and the final velocity and the minimal velocity are predicted equal to 0.1 mm/s and -0.024 mm/s. Thus, according to the analysis in section 3(B), the system may run stably and appears creep. This point will be further verified with the simulation using these actual parameters. This simulation result is shown in Fig. 7. From this Figure, it is clear that the system runs stably and appears creep, and the final velocity and the minimal velocity are equal to 0.1 mm/s and -0.02 mm/s, respectively.

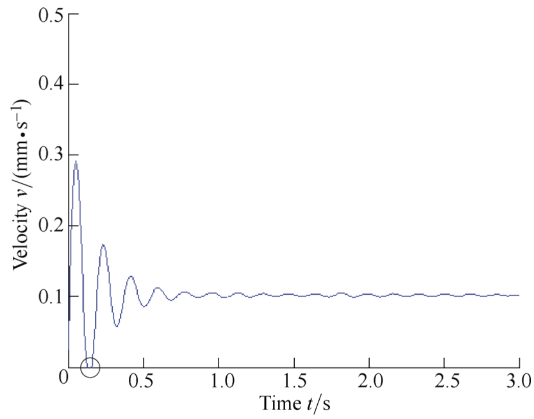

Fig. 7. Stable run and creep at $\xi>1$

(4) Result verification at $\xi=1$

The simulation parameters are set as $\{x(0)=0$, $v(0)=1\times10^{-3}$ m/s, $F_d(0)=1.359\times10^{7}$ N, $v_s=2.223\ 9\times10^{-3}$ m/s, $F_2=1.003\times10^{7}$ N, $Q=18\times10^{-4}$ m^3/s, $n=2.1$, $u_s=0.95$, $c=0.460\ 9$, $m=0.12$, $y=96.65\}$. By calculation, ξ is equal to 1, and the final velocity and the maximal overshoot are predicted equal to 1 mm/s and 1.6 mm/s, respectively. Thus, according to the analysis result in section 3(C), the system may run stably and does not appear creep. This point will be further verified with the simulation using these actual parameters. This simulation result is shown in Fig. 8, which shows that the system runs stably, the final velocity and the maximal overshoot are predicted equal to 0.99 mm/s and 1.59 mm/s, respectively.

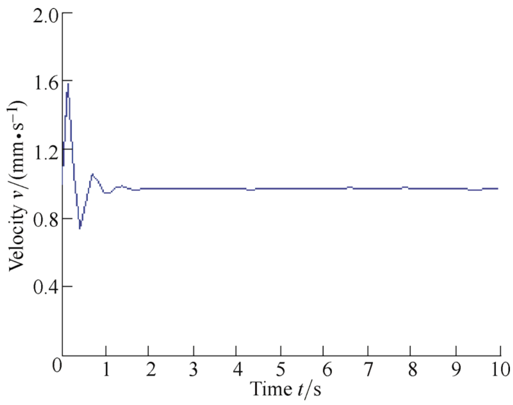

Fig. 8. Stable run at ξ=1

4.2 Experiment verification

An experiment on the practical 4000T HPM is used to verify the effectiveness of these derived results. The schematic of the experimental setup is shown in Fig. 9. The entire system is powered by a pump station. The oil pressures of three driving cylinders located above the work plate are controlled by servovalves. These servovalves receive control signals from a control panel equipped with a PC, a PLC (SIMATICS7-300) and a data acquisition board for pressure, displacement and velocity measurement. The pressure data are collected using the pressure sensors installed at the inlet of the driven cylinders. The displacement sensors are installed at the vertical columns. In this verification, a long rectangular aluminum alloy work piece is forged. The work pieces at the before- and after-forged are shown in Figs. 10(a) and 10(b), respectively.

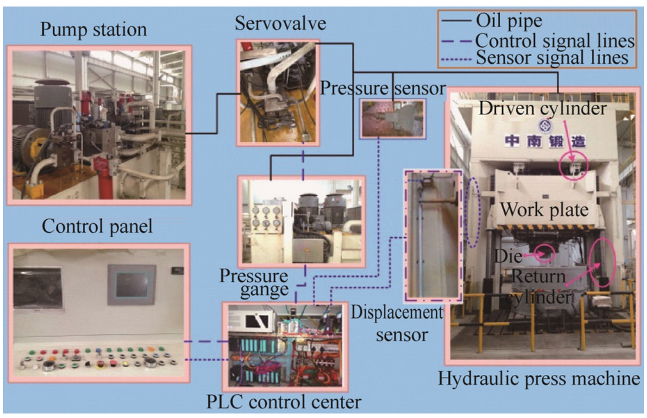

Fig. 9. Practical 4000T HPM

(a) Initial shape

(b) Final shape

Fig. 10. Work piece at the before- and after-forged

In this experiment, the pressure is shown in Fig. 11(a). According to the practical or calculated parameters in Table 1 and Eqs. (7), (8), and (10), the parameter ξ is calculated equal to 0.029 2, and the final velocity and the maximal overshoot are estimated equal to 0.1 mm/s and 0.162 mm/s, respectively. This system should run in a stable condition according to the analysis result in the section 3(A). The practical velocity response in the Fig. 11(b) clearly checks this point since it can run stably around 0.095 mm/s and its maximal overshoot is equal to 0.148 mm/s. Thus, this performance analysis is effective.

Table 1. System parameters

Description	Value
Mass of work plate M/kg	54 474
Area sum of hydraulic cylinders A/m^2	0.53
Viscous damping coefficient B/(N • (m • s^{-1})$^{-1}$)	6.85×10^5
Spring moment of medium β_e/(N • m^{-2})	0.7×10^9
Initial volume V_0/m^3	3
Stribeck velocity v_s/(m • s^{-1})	0.5×10^{-3}
Static friction value F_s/N	11 742.98
Coulomb friction value F_c/N	10 419.54
Friction coefficient σ_2/(N • (m • s^{-1})$^{-1}$)	82 298.41
Parameter K_{zx}	1×10^5
Parameter K_{zv}	3.602×10^5

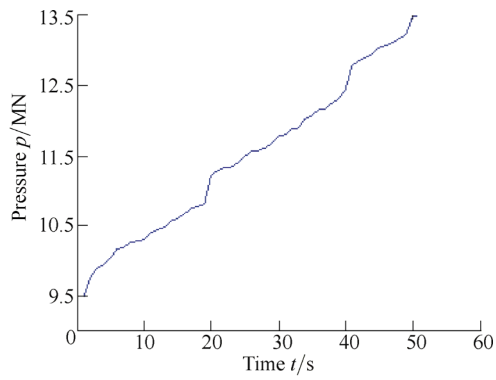

(a) Pressure

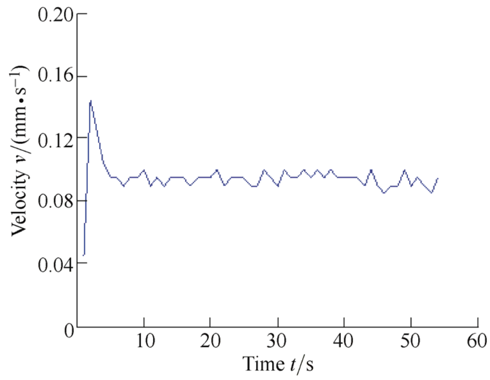

(b) Velocity

Fig. 11. Forging response

5 Conclusions

(1) An approximate model based dynamic response estimation method is proposed for the high-quality forging. It is an effective solution to achieve the desirable low-velocity forging condition.

(2) The developed approximate model can represent the system response well at low-velocity working point. This may greatly ease the complexity of the estimation of the

dynamic response.

(3) The dynamic responses of the forging process can be predicted well. The conditions for stability, vibration, and creep are also derived effectively, which will benefit the design of the controller for a satisfactory dynamic performance.

(4) The correctness of all analytical results has been confirmed by both experiment and simulations.

References

[1] CHEN Hua. Effect of forging process parameters on re-crystallization behavior of 7050 aluminum alloy[J]. *Aluminum Fabrication*, 2007, 3(175): 33–35. (in Chinese)

[2] LIANG Xin, CHEN Kanghua, CHEN Xuehai, at al. Effect of isothermal forging rate on microstructure and properties of 7085 aluminum alloy[J]. *Materials Science and Engineering of Powder Metallurgy*, 2011, 16(2): 290–295.

[3] SHEN Gang-shu, FURRER D. Manufacturing of aerospace forgings[J]. *Journal of Materials Processing Technology*, 2000, 98(2): 189–195.

[4] LU Xinjiang, HUANG Minghui. Multi-domain modeling based robust design for nonlinear manufacture system[J]. *International Journal of Mechanical Sciences*, 2013, 75: 80–86.

[5] BEDDOES J, BIBBLY M. *Principles of metal manufacturing process*[M]. Oxford: Butterworth-Heinemann, 1999.

[6] LIN Z P, *Engineering computation of deformation force under forging*[M]. Beijing: Mechanical Industry Press, 1986. (in Chinese)

[7] BOER C R, REBELO N, RYDSTAD H, et al. *Process modelling of metal forming and thermomechanical treatment*[M]. New York: Springer-Verlag, 1985.

[8] HUANG Shunzhou, ZHAO Yong, WANG Hao, at al. Stabilized multi-domain simulation algorithms and their application in simulation platform for forging manipulator[J]. *Chinese Journal of Mechanical Engineering*, 2014, 27(1): 92–101.

[9] OWEN W S, CROFT E A. The reduction of stick-slip friction in hydraulic actuators[J]. *IEEE/ASME Transactions on Mechatronics*, 2003, 8(3): 362–371.

[10] LIN C J, YAU H T, TIAN Y C. Identification and compensation of nonlinear friction characteristics and precision control for a linear motor stage[J]. *IEEE/ASME Transactions on Mechatronics*, 2013, 18(4): 1385–1396.

[11] LEE T H, TAN K K, HUANG S. Adaptive friction compensation with a dynamical friction model[J]. *IEEE/ASME Transactions on Mechatronics*, 2011, 16(1): 133–140.

[12] MOSTEFAI L, DENA M, HORI Y. Robust tracking controller design with uncertain friction compensation based on a local modeling approach[J]. *IEEE/ASME Transactions on Mechatronics*, 2010, 15(5): 746–756.

[13] SEPEHRI N. Simulation and experimental studies of gear backlash and stick-slip friction in hydraulic excavator swing motion[J], *Journal of Dynamic Systems, Measurement, and Control*, 1996, 118(3): 463–467.

[14] ZHANG Pu, YAO Zhenqiang, DU Zhengchun. Impedance analysis of forging process and strategy study on compliance for forging manipulator[J]. *Chinese Journal of Mechanical Engineering*, 2013, 26(4): 651–658.

[15] SOUZA Jr O H, BARBIERI N, SANTOS A H M. Study of hydraulic transients in hydropower plants through simulation of nonlinear model of penstock and hydraulic turbine model[J]. *IEEE Transactions on Power Systems*, 1999, 14(4): 1269–1272.

[16] HUANG Minghui, LI Yibo, ZHANG Meng, at al. Dynamic performance analysis for die-forging press machine under extremely low speed[J]. *Journal of Central South University (Science and Technology)*, 2012, 43(11): 4259–4267. (in Chinese)

[17] MOKHTAR M O A, YOUNES Y K, EL MAHDY T H, et al. A theoretical and experimental study on the dynamics of sliding bodies with dry conformal contacts[J]. *Wear*, 1998, 218(2): 172–178.

[18] MURAKI M, KINBARA E, KONISHI T. A laboratory simulation for stick-slip phenomena on the hydraulic cylinder of a construction machine[J]. *Tribology International*, 2003, 36(10): 739–744.

[19] CAPONE G, D'AGOSTINO V, VALLE S D, et al. Influence of the variation between static and kinetic friction on stick-slip instability[J]. *Wear*, 1993, 161(1–2): 121–126.

[20] XIE Jingjing. *Low-speed performance analysis and control strategy for large scale forging press*[D]. Changsha: Central South University, 2014. (in Chinese)

[21] LU Xinjiang, HUANG Minghui. System decomposition based multi-level control for hydraulic press machine[J]. *IEEE Tran. On Industrial Electronics*, 2012, 59(4): 1980–1987.

[22] Liu Huihui. *Stability of steady sliding with velocity dependent and LuGre type friction model*[D]. Xi'an: Xi'an University of Technology, 2008. (in Chinese)

Biographical notes

LEI Jei, born in 1988, is currently a graduate student at *School of Mechanical & Electrical Engineering, Central South University, China*. His interests include large die forging equipment.
Tel: +86-15111256871; E-mail: 133711018@csu.edu.cn

LU Xinjiang is currently an associate professor at *School of Mechanical & Electrical Engineering, Central South University, China.* His research interests include system design, process modeling and control, robust design, and integration of design and control.
E-mail: luxj@csu.edu.cn

LI Yibo, born in 1981, is currently a lecturer at *School of Mechanical & Electrical Engineering, Central South University, China.*
E-mail: liyibo@csu.edu.cn

HUANG Minghui is currently a professor at *School of Mechanical & Electrical Engineering, Central South University, China.* His research interests include machine design and manufacturing, design theory, fault diagnosis, and digital manufacturing.
E-mail: meeh@mail.csu.edu.cn

ZOU Wei, born in 1992, is currently a graduate student at *School of Mechanical & Electrical Engineering, Central South University, China.*
E-mail: 258374202@qq.com